

Gamma-ray burst Jet Progenitor: long vs short bursts by angular momentum and mass ratio

She-Sheng Xue

ICRANet Piazzale della Repubblica, 10 -65122, Pescara, Italy
Physics Department, Sapienza University of Rome, Rome, Italy
INFN, Sezione di Perugia, Perugia, Italy
ICTP-AP, University of Chinese Academy of Sciences, Beijing, China

E-mail: xue@icra.it, she-sheng.xue@cern.ch

Abstract. In this study, we investigate the homologous collapse dynamics of a slowly rotating stellar nuclear core. We incorporate the virial theorem of hadron collisional relaxations to analyze the conversion of gravitational potential energy into kinetic energy of hadrons. Additionally, we consider the production of photons and electron-positron pairs resulting from hadron collisions. Our analysis reveals a gravo-thermal process wherein gravitational energy transforms into energy associated with photons and pairs. The presence of axial symmetric centrifugal potential reduces the gravitational potential energy gain. The presence of axial symmetric centrifugal potential mitigates the gain in gravitational potential energy. Consequently, we observe the formation of highly energetic and opaque photon-pair jets, whose size, peak spectra, energy and number densities are consistent with observed energetic features and empirical relationships of Gamma-Ray Burst (GRB) progenitors. Furthermore, we find that the angular momentum and mass ratio (J/M) of the collapsing core and binary coalescence play crucial roles in determining the jet angle and the differentiation between short and long bursts. Our findings contribute to a deeper understanding of the mechanisms governing GRBs' progenitor systems.

Contents

1	Introduction	2
2	Adiabatic approximation in gravitational collapse	2
3	Virial theorem and gravo-thermal configuration	3
4	Photon production from hadron collisions	4
5	Gravitational collapse of rotating stellar cores	5
5.1	Static equilibrium configuration	6
5.2	Homologous collapse of rigid rotating core	7
5.3	Spherical and homologous solution in space	8
5.4	Initial central density and length scale function in time	9
5.5	Core mass and angular momentum conservations	11
6	Photon-pair sphere/jet energetic properties	12
6.1	Photon-pair sphere/jet temperature profiles	12
6.2	Photon-pair sphere/jet density and size profiles	13
6.3	Photon-pair sphere/jet energy and spectrum peak	14
7	Long vs short GRBs by angular momentum and mass ratio	16
7.1	Trends of jet features varying with J/M	16
7.2	A separatrix in angular momentum J/M	17
7.3	Long vs short GRBs	18
8	Conclusion and remarks	19

1 Introduction

Gamma-ray bursts (GRBs) are the most energetic and complex events in the Universe. Within mere seconds, their progenitors release high-energy photons of tremendous energy ranging from 10^{49} to 10^{54} ergs. Despite significant advancements in our comprehension of GRBs, achieved through extensive research efforts [1–7], a fundamental question remains unanswered: what are the dominant dynamics of GRB progenitors that ultimately yield the formation of an energetic and optically thick plasma composed of photons and electron-positron pairs, i.e., a fireball or jet? Massive stellar gravitational potentials are indeed vast reservoirs of energy, and during stellar collapse and coalescence, significant amounts of gravitational energy are released. The critical question is how this immense gravitational energy is converted into photon and pair energies within just a few seconds during GRBs.

In a self-gravitating system, Lynden-Bell and Wood [8, 9] pioneered the study of gravo-thermal catastrophe using the framework of violent hadron collisionless relaxation and the virial theorem. Their work demonstrated the relaxation process in which hadrons gain their mean kinetic heat energy from gravitational potential energy.

On the other hand, the production of photons by hadron collisions has been extensively studied in the context of heavy-ion collisions [10–15]. Based on the homologous core collapse scenario [16], we show that hadrons gain gravitational energy through collisional relaxation. Hadron-hadron collisions subsequently produce photons, leading to the conversion of gravitational energy into the energies of opaque photon-pair spheres. This process accounts for the origins of GRBs’ energies and their empirical correlations [17].

Furthermore, we investigate the formation of photon-pair jets in scenarios involving rotating core collapse and binary coalescence. We find that the angular momenta and mass ratios of these systems determine the jet angle and the distinct characteristics of long versus short GRBs.

We organize this article as follows. Based on the adiabatic assumption, Sections 2, 3, and 4 present discussions on gravo-thermal catastrophe, the virial theorem, and photon production from hadron relaxations and collisions. In Section 5, we discuss the homologous collapse of a slowly rotating core. Sections 6 and 7 study the properties and correlations of photon-pair spheres and jets. The characteristics of long versus short GRBs, as determined by progenitor angular momenta and mass ratios, are described in Sections 7 and 8.

The stellar core density is characterised by the nuclear saturation density $n_0 \approx 0.16 \text{ fm}^{-3} = 1.6 \times 10^{38} / \text{cm}^3$ or $\rho_0 = mn_0 \approx 2.4 \times 10^{35} \text{ ergs/cm}^3$, and $m \approx 1 \text{ GeV}$ is the typical baryon (neutron) mass. The light speed $c = 1$, Planck constant $\hbar = 1$ and Boltzmann constant $k = 1$ are used unless otherwise specified.

2 Adiabatic approximation in gravitational collapse

Gravitational collapse is a dynamic avalanche involving complex microscopic and macroscopic processes occurring at vastly different scales. It is challenging for both analytical

and numerical approaches to analyze all these dynamics without any approximations. To make appropriate approximations, we need to understand the dominant physical processes and their variations across the relevant length and time scales.

We consider a rotating stellar core of mass M , radius R , and angular velocity Ω undergoing a gravitational collapse process. The most relevant timescales τ_{grav} are collapsing $|R|/|\dot{R}|$, rotating $1/\Omega$ and hydrodynamics timescale $\sim R/v_s$, where v_s is the sound velocity. These macroscopic scales are much larger than the microscopic scales of baryon collisional relaxation, photon production, and thermalization.

This disparity in scales implies that:

- these microscopic processes occur not only “instantaneously” but also “locally” compared with gravitational collapsing and hydrodynamic processes.
- There is no causal correlation among the concurrent microscopic processes at different space-time points on macroscopic scales.

In other words, the vast difference between microscopic and macroscopic timescales suggests that gravitational collapse can be considered a very slow, *adiabatic* process compared to these rapid and local microscopic processes. Therefore, these microscopic processes can be approximately analyzed as if the self-gravitating cores were static.

Based on this adiabatic approximation, we discuss isothermal configurations during gravitational collapses.

3 Virial theorem and gravo-thermal configuration

We consider a stellar core composed of N baryons of mass m ¹. In gravitational collapse, baryons gain their mean kinetic energy F from the gravitational energy U via collisionless relaxation. This gravo-thermal catastrophe phenomenon of stellar cores is studied by considering violent relaxation [8] and equipartition theorem [9]. In these studies, the stellar core is an isothermal core of baryon temperature $T \ll m$ and internal “heat” energy $F = \frac{3}{2}TN$. It is an equilibrium or equipartition system, where the Clausius virial theorem applies,

$$2F + U + U_c = 3PV, \quad (3.1)$$

where V is the core volume, and P is the external pressure acting on the core surface. Here, $U_c \ll U$ represents the centrifugal potential energy for a slowly rotating core, which we will further justify.

These studies indicate that the baryon collisionless relaxation process in gravitational potential and under external pressure leads to two key consequences:

- The gravitational energy is converted to the internal heat energy of baryons.

¹By the term *baryons*, we indicate nucleons, nuclei, hadrons, quark-gluon plasma that carry baryon numbers.

- The balance between gravitational dynamics and thermodynamics is established, making the virial theorem (3.1) applicable.

The second point holds, provided the time scales of microscopic relaxation processes are much smaller than those of macroscopic gravitational and hydrodynamical processes, justifying adiabatic approximation. Following the discussions in the pioneer works [18, 19], it is noted that the gravitational evolution time scale due to stellar evaporation and consumption is longer than the core relaxation time scale, the core will maintain an approximate isothermal core profile (3.1) and evolve homologously.

We generalise these discussions to a small fluid element of volume dV inside the stellar core. Given that the baryon-baryon collision timescale at nuclear density is small, equipartition or equilibrium can be locally achieved through the relaxation processes of baryon-baryon collisions. The *local* virial theorem (3.1) is given by [17]

$$2dF + dU + dU_c = 3pdV, \quad (3.2)$$

and $dF = (3/2)T(\rho/m)dV$, $dU = (1/2)\rho\phi dV$ and $dU_c = \phi_c\rho dV$. Here baryon mass density $\rho = mn$ and number density n . The terms ϕ and ϕ_c are gravitational and centrifugal potential in a rotating frame, respectively. For each fluid element of mass energy ρdV , the baryon temperature T characterises the mean kinetic energy dF of baryon motions and collisions, $dF \ll \rho dV$ for $T \ll m$. The fluid element's rotating energy is much smaller than its gravitational energy, i.e., $dU_c \ll |dU|$. For an isothermal core, integrating Eq. (3.2) over the core volume $\int dV$, one obtains the virial theorem (3.1), using $\int pdV = PV$. This shows that the local equilibrium properties extend to the entire core under the adiabatic approximation.

Moreover, we approximately describe the internal pressure p by the polytropic equation of state (EoS)

$$p = \kappa\rho^\gamma, \quad (3.3)$$

with two parameters: mean thermal index γ and coefficient κ . As a result, combining the local virial theorem (3.2) and the EoS (3.3), we obtain the baryon temperature:

$$3T/m \approx 3v_s^2(1/\gamma) - (1/2)\phi - \phi_c, \quad (3.4)$$

where v_s is the sound velocity given by,

$$v_s^2 = \partial p / \partial \rho = \gamma p / \rho. \quad (3.5)$$

This relationship shows that via collisional relaxations, baryons gain heat energy (temperature) from the gravitational potential, which is effectively reduced by the centrifugal potential.

4 Photon production from hadron collisions

The baryon-baryon collisions produce photons and pairs of light-charged leptons and quarks. Consequently, the mean kinetic heat energy of baryons is converted to the

energy of photons, and pairs of other light-charged leptons and quarks. From the studies of heavy-ion collisions [10, 11, 11, 12, 12–15], we learn about photon production in these collisions and can obtain the photon number and energy densities as follow [17],

$$n_\gamma \approx \frac{4}{3} \frac{\alpha \alpha_s}{\pi} T^3 \ln \left(1 + \frac{2.9}{4\pi \alpha_s} \right), \quad (4.1)$$

$$\rho_\gamma \approx \frac{8}{3} \frac{\alpha \alpha_s}{\pi} T^4 \ln \left(1 + \frac{2.9}{4\pi \alpha_s} \right), \quad (4.2)$$

where $\alpha = 1/137$. The QCD coupling $\alpha_s \approx 0.5$ indicates that the photon production described by equation (4.2) is dominant over other QED processes producing photons.

The gravo-thermal catastrophe produces not only heat energy for massive baryons, given by $(3/2)T(\rho/m)dV$ (as in equation (3.2)), but also energy for relativistic particles, described by $\rho_\gamma dV$ (as in equation (4.2)). For a baryon temperature T on the order of $\mathcal{O}(10^2)$ MeV, the photon density n_γ (as in equation (4.2)) is so large that relativistic particles become opaque and thermalized by collisions among themselves. The mean temperature T_γ of thermalized photons can be estimated by equating photon thermal energy density to that given in equation (4.2)

$$\frac{\pi^2}{15} T_\gamma^4 \approx \rho_\gamma, \quad \Rightarrow \quad T_\gamma \approx 0.21T. \quad (4.3)$$

Moreover, these photons couple to pairs of charged leptons (quarks) and anti-leptons (-quarks). Among these charged particle pairs, we consider pairs of electrons and positrons since their masses are smaller than the photon characteristic energy given in equation (4.3). Therefore, the fourth and back processes involving the production and annihilation of electron-positron pairs, $\gamma + \gamma \leftrightarrow e^+ + e^-$, are kinematically possible. The cross-section $\sigma_{\gamma\gamma \leftrightarrow e^+e^-}$ is of the order of the Thomson cross section σ_γ , and the corresponding mean-free length is given by $\sim (\sigma_{\gamma\gamma \leftrightarrow e^+e^-} n_\gamma)^{-1}$, which is very small. This indicates that via processes $\gamma + \gamma \leftrightarrow e^+ + e^-$, photons and electron-positron pairs participate in thermalisation or thermal equipartition in particle energy and number. As a result, these processes lead to an electrically neutral, deeply opaque, and thermalised plasma (fluid) of photons and electron-positron pairs.

As a consequence, the isothermal core profile is approximately described by baryon temperature T (equation (3.4)) and photon temperature T_γ (equation (4.3)), as well as the photon production number and energy densities (equations (4.1) and (4.2)). The core will maintain this isothermal profile and evolve homologously.

5 Gravitational collapse of rotating stellar cores

Observations of neutron stars, supernovas, and GRBs suggest that rotation is crucial in the core collapse scenario. However, there is still a lack of realistic models for the final evolutionary state of a massive collapsing star that consistently includes rotation. We proceed along the lines of previous Newtonian and rotating core collapse studies, which construct a set of differentially rotating polytropes in equilibrium as pre-collapse iron core models [20, 21].

We consider a slowly rotating stellar core undergoing a gravitational collapse process, whose rotation energy is much smaller than gravitational energy. In the Newtonian approximation, we describe the process by the continuity equation for the baryon number conservation, Euler's equation for energy-momentum conservation, Poisson's equation for gravitational potential ϕ are,

$$\frac{\partial \rho}{\partial t} + \nabla \cdot (\rho \mathbf{u}) = 0, \quad (5.1)$$

$$\left(\frac{\partial \mathbf{u}}{\partial t}\right) + \nabla \left(\frac{1}{2}|\mathbf{u}|^2\right) + (\nabla \times \mathbf{u}) \times \mathbf{u} + \nabla h + \nabla \phi + \nabla \phi_c = 0, \quad (5.2)$$

$$\nabla^2 \phi - 4\pi G \rho = 0, \quad (5.3)$$

where baryon fluid is described by density ρ and velocity \mathbf{u} . Equation of State (3.3) yields the baryon heat function $h = H/\rho$ (H for Enthalpy)

$$\nabla h = \nabla p/\rho; \quad h = \int \nabla p/\rho = \frac{\kappa\gamma}{\gamma-1} \rho^{\gamma-1}. \quad (5.4)$$

We formally add the gradient of centrifugal potential ϕ_c given by $\nabla \phi_c = j \nabla \Omega$, where j and Ω are angular momentum and velocity respectively. These equations reduce to their counterparts in the hydrodynamic equilibrium case, describing the core's state when the dynamic effects of collapse are not present.

5.1 Static equilibrium configuration

To develop a simple analytical model for a rigidly rotating stellar core undergoing gravitational homologous collapse, we start with the established equilibrium conditions and rotation laws. In hydrodynamic equilibrium, the integrability condition of Euler's equation (5.2) necessitates that the angular momentum j depends only on angular velocity Ω . We adopt the rotation law from Refs. [22–24],

$$j = A^2(\Omega_c - \Omega), \quad (5.5)$$

where Ω_c is the value at the centre of the coordinate. The rotation parameter A is a positive constant (length scale), which implicitly depends on Ω_c .

In the Newtonian approximation, the rotation law simplifies to

$$\begin{aligned} \Omega &\approx \Omega_c/(1 + x^2/A^2), \quad j \approx x^2\Omega, \\ \phi_c &= \int j d\Omega \approx A^2 x^2 \Omega/2 + \text{const}, \end{aligned} \quad (5.6)$$

where $x = R \sin \theta$ and $z = R \cos \theta$ are the cylindrical coordinates, R is the radial coordinate, and θ is the zenith (polar) angle. The rotating axis is along the \hat{z} direction.

We focus on the limit of constant angular velocity, namely a rigid rotating core. In this limit,

$$\Omega \rightarrow \Omega_c, \quad x^2/A^2 \ll 1, \quad (5.7)$$

and up to the leading order $\mathcal{O}(x^2/A^2)$,

$$j \approx x^2 \Omega_c, \quad \phi_c \approx \frac{A^2 x^2 \Omega_c}{2}. \quad (5.8)$$

We set the centrifugal potential to zero at the rotating axis $x = 0$, thus ensuring that $\phi_c = 0$ at $x = 0$.

In the static equilibrium case, integrating Euler's equation (5.2) yields

$$h + \phi + \phi_c = \text{constant}, \quad (5.9)$$

which is uniform across the space.

To generalize this to a model of a rigidly and slowly rotating stellar core undergoing homologous collapse, we need to consider the density, velocity, and potential changes during the collapse. Given the homologous nature of the collapse, the density profile remains similar while scaling with time.

5.2 Homologous collapse of rigid rotating core

To analyze the homologous collapse of a nearly spherically symmetric, rigidly and slowly rotating stellar baryon core, we follow the approach of Goldreich and Weber [16] in the rotating frame. We assume the baryon fluid flow is vorticity-free, meaning $(\nabla \times \mathbf{u}) = 0$. The velocity $\mathbf{u} = \nabla v$ can thus be expressed as a gradient of a scalar function v :

$$\mathbf{u} = \nabla v, \quad v = (1/2)(\dot{a}/a)R^2, \quad \mathbf{u} = (\dot{a}/a)\mathbf{R} = \dot{a}\mathbf{r}. \quad (5.10)$$

Here, $a(t)$ is a length scale function, and \mathbf{R} is the radial vector in the physical coordinates. The core density ρ and sound velocity v_s (3.5) in the core can be expressed in terms of a homologous function $f(r)$,

$$\rho = \rho_c f^3, \quad v_s^2 = \gamma p / \rho = (v_s^c)^2 f^{3(\gamma-1)}, \quad (5.11)$$

where r is the dimensionless radius

$$r = R/a(t), \quad \mathbf{r} = \mathbf{R}/a(t). \quad (5.12)$$

Here ρ_c is the central density, and v_s^c is the central sound velocity, given by $(v_s^c)^2 \equiv \gamma p_c / \rho_c$. The length scale function $a(t)$ relates to the central density and sound velocity by:

$$a(t) = v_s^c / (\gamma \pi G \rho_c)^{1/2}. \quad (5.13)$$

Given the functional forms of ρ and \mathbf{u} , the continuity equation (5.1) reduces to the trivial relation $\dot{f} = 0$, indicating that the homologous profile $f(r)$ is time-independent. The integrated Euler equation (5.2) yields

$$\frac{\partial v}{\partial t} + \frac{1}{2} |\nabla v|^2 + h + \phi + \phi_c = \text{constant}, \quad (5.14)$$

which reduces to the equation (5.9) in the static equilibrium case $\dot{a} = 0$ and $v = 0$.

We are now in the position of postulating the rotation law for a rigidly and slowly rotating stellar core, which undergoes homologous gravitational collapse. Since the stellar rotating scale Ω^{-1} and collapsing timescales $\tau_{\text{grav}} = R/\dot{R}$ are much larger than microscopic interaction and thermalization timescales, we approximately consider the gravitational collapse of rotating stellar core is an adiabatic process. Namely, at each collapse step at time t , the stellar core is approximately in an equilibrium state as if the collapsing stellar core adiabatically evolves in a time sequence of equilibrium states during gravitational collapse. The rigid core angular velocity $\Omega(t)$ increases in time. Therefore, we generalize the equilibrium rotation law (5.6) to

$$j(t) = r^2 \sin^2 \theta a^2(t) \Omega(t); \quad \phi_c(t) = \frac{A^2(t)}{2} r^2 \sin^2 \theta a^2(t) \Omega(t), \quad (5.15)$$

where $A(t)$ is the time-dependent rotation parameter.

To further describe the centrifugal potential ϕ_c of a slowly and rigidly rotating, homologously collapsing stellar core, we assume a time-dependent rotation parameter $A(t)$ in (5.15) depends on the centre sound velocity

$$A^2(t) = \mathcal{A}^2 [v_s^c(t)]^2, \quad (5.16)$$

and \mathcal{A} is a constant that does not depend on time. Thus, the centrifugal potential of a slowly and rigidly rotating and homologous collapsing core can be expressed by

$$\phi_c = \frac{[v_s^c(t)]^2}{2} r^2 \sin^2 \theta \mathcal{A}^2 a^2 \Omega, \quad \mathcal{A}^2 a^2 \Omega = \mathcal{A}^2 a^2(t) \Omega(t), \quad (5.17)$$

in the rotating frame. We will show soon that $\mathcal{A} a^2 \Omega = \mathcal{A} a^2(t) \Omega(t)$ is time-independent, based on total core mass and angular momentum conservation.

By integrating these equations, the evolution of the collapsing core can be numerically simulated or approximately analyzed, incorporating the effects of rotation and centrifugal potential. This approach can yield insights into the final state of the collapsing core, and help understand phenomena such as supernovae and gamma-ray bursts.

5.3 Spherical and homologous solution in space

Using the ansatz $v = (1/2)(\dot{a}/a)R^2$, Euler's equation (5.14) is separable in spatial and temporal variables,

$$h + \phi = \frac{(v_s^c)^2}{\gamma - 1} \frac{\lambda}{6} r^2, \quad (5.18)$$

$$a^{\frac{\gamma}{2-\gamma}} \ddot{a} = -\frac{\lambda}{6} \frac{2\gamma}{\gamma - 1} \left(\frac{\kappa^{\frac{1}{\gamma-1}}}{\pi G} \right)^{\frac{\gamma-1}{2-\gamma}}. \quad (5.19)$$

where the positive eigenvalue λ relates to the material binding energy of baryon fluid per energy density ρ [16] or external pressure acting on the core surface. The core

outer radius r_s decreases as the λ value increases. Equation (5.19) describes the time evolution of the length scale function $a(t)$ in the collapsing core.

The spatial solution to the Euler's equation (5.18) is

$$h = \frac{(v_s^c)^2}{\gamma - 1} f^{3(\gamma-1)}, \quad \phi = \frac{(v_s^c)^2}{\gamma - 1} \left(\frac{\lambda}{6} r^2 - f^{3(\gamma-1)} \right). \quad (5.20)$$

Poisson's equation (5.3) yields a second-order differential equation,

$$\frac{1}{r^2} \frac{d}{dr} \left(r^2 \frac{df^{3(\gamma-1)}}{dr} \right) + \frac{4(\gamma - 1)}{\gamma} f^3 = \lambda, \quad (5.21)$$

the boundary conditions are $f'(0) = 0$ and $f(0) = 1$. Following [16] for the $\gamma = 4/3$ solution, we obtain general solutions for $1 < \gamma < 4/3$ [17]. As shown in Fig. 1, three solutions of homologous density profile f^3 correspond to the selected values (γ, λ) :

solutions	γ	λ	r_s
orange	1.24	1.0×10^{-4}	23
blue	1.23	8.0×10^{-5}	36
green	1.225	8.0×10^{-6}	34

(5.22)

The homologous profile $f(r)$ becomes tangent to $f = 0$ at the core outer radius r_s , namely $f'(r_s) \approx 0$. The core homologous profile $f(r)$ and outer radius r_s do not depend on time.

In our analysis, we approximately decouple the centrifugal potential ϕ_c from the Euler equation (5.14), because the rotational potential energy is much smaller than the heat and gravitational potential energies. Namely, we neglect the back-reaction dynamics of the rotation potential ϕ_c in homologous gravitational collapse. The gravitational potential ϕ and heat function h are balanced with the λ term in Eq. 5.18. The homologously collapsing cores remain spherically symmetric without high moments.

The hydrodynamics of slow-rotating core collapse up until the core bounce can be understood in this relatively simple analytic model. This model provides a framework for understanding the centrifugal potential of a slowly and rigidly rotating core collapse until the core bounces, laying the groundwork for more detailed numerical simulations or further analytical refinements.

5.4 Initial central density and length scale function in time

The temporal equation (5.19) governs how the scale length $a(t)$ changes in time, and the solution is

$$\frac{a(t)}{a_{\min}} = \left\{ 1 + \left[\frac{\lambda \gamma}{3(2 - \gamma)(\gamma - 1)^2} \right]^{\frac{1}{2}} \left(\frac{t}{\tau_{\min}} \right) \right\}^{2-\gamma}. \quad (5.23)$$

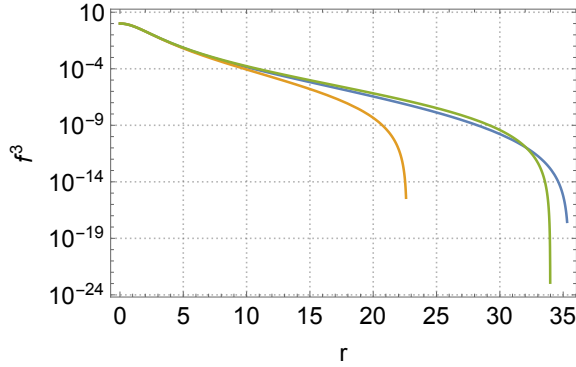


Figure 1. Colours on line for different eigenvalues (5.22). We show numerical solutions to the eigenvalue problem of Eqs. (5.18) and (5.19). The homologous density profile f^3 is plotted as a function of dimensionless radius $r = R/a$. The density profile f^3 does not change in time and vanishes at the core outer radius r_s (5.22).

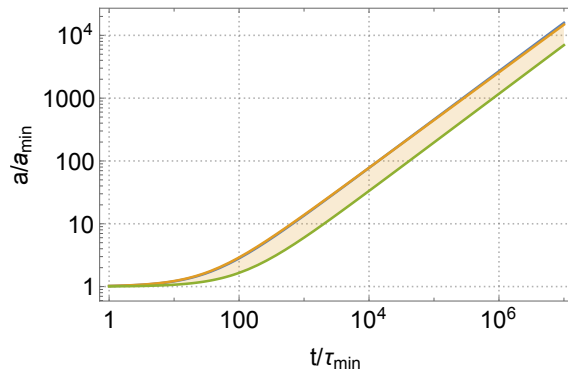


Figure 2. Corresponding to the density profile f^3 in Fig. 1, the scale length $a(t)/a_{\min}$ is plotted as in terms of t/τ_{\min} , using units a_{\min} (5.24) and τ_{\min} (5.25). Note that the initial time $t_{\text{initial}} \sim 10^7 \tau_{\min} \sim \mathcal{O}(1)$ second, given by the initial conditions (5.27). The shadow in between these colour lines indicates other possible physical solutions.

In a collapsing process from the initial time t_{initial} to the final time $t_{\text{final}} = \tau_{\min}$, the scale function $a(t)$ decreases significantly, approaching the minimum,

$$a_{\min} = (3\gamma)^{\frac{2-\gamma}{2(\gamma-1)}} \left(\frac{\kappa}{\pi G} \right)^{1/2} = 3.06 \times 10^5 (3\gamma)^{-1/2} \left(\frac{\rho_c^{\max}}{\rho_0} \right)^{-1/2} (\text{cm}). \quad (5.24)$$

$$\tau_{\min} \equiv \left(\frac{1}{\pi G \rho_c^{\max}} \right)^{1/2} = 1.02 \times 10^{-5} \left(\frac{\rho_c^{\max}}{\rho_0} \right)^{-1/2} (\text{sec}), \quad (5.25)$$

and $\tau_{\min} = (3\gamma)^{1/2} a_{\min}$. It gives the basic macroscopic length scale of the homologous collapse. The centre density ρ_c and sound velocity v_s^c increase in time,

$$\rho_c = \rho_c^{\max} \left(\frac{a}{a_{\min}} \right)^{-\frac{2}{2-\gamma}}; \quad (v_s^c)^2 = \frac{1}{3} \left(\frac{a}{a_{\min}} \right)^{-\frac{2\gamma-1}{2-\gamma}} = \frac{1}{3} \left(\frac{\rho_c}{\rho_c^{\max}} \right)^{\gamma-1}, \quad (5.26)$$

approaching their maximal values $\rho_c^{\max} = (3\gamma\kappa)^{-\frac{1}{\gamma-1}}$ and $1/\sqrt{3}$. The maximal centre density $\rho_c^{\max} = (3\gamma\kappa)^{-\frac{1}{\gamma-1}}$ is about 10 times the nuclear saturation energy density $\rho_0 \approx 2.4 \times 10^{35} \text{ergs/cm}^3$, corresponding to the number density $n_0 \approx 1.6 \times 10^{38} \text{/cm}^3$.

Instead of using collapsing time t , we choose the central density $\rho_c(t)$ as the primary variable to describe the homologous gravitational collapse of a stellar core. This choice is physically intuitive and aligns with the key stages of the collapse, characterized by changes in the core density. The initial value $\rho_c^{\text{in}} = \rho_c(t_{\text{initial}})$ depends on the homologous core mass M and radius r_s . From Eqs. (5.23-5.26), we obtain

$$\rho_c^{\text{in}} \sim 10^{-6} \rho_c^{\max} \quad (5.27)$$

for $t_{\text{initial}} \sim 10^6 \tau_{\text{min}} \sim \mathcal{O}(1)$ seconds. The final value $\rho_c^{\text{fi}} = \rho_c(t_{\text{final}})$ is the maximal value ρ_c^{\max} . The core undergoes a homologous collapsing process: starting from the initial time $t_{\text{initial}} \sim \mathcal{O}(1)$ seconds and initial core centre density ρ_c^{in} , ending at the final time $t_{\text{final}} = \tau_{\text{min}} \sim 10^{-5}$ seconds and final core centre density is $\rho_c^{\max} \approx 10\rho_0$. The duration is about $\mathcal{O}(1)$ seconds.

5.5 Core mass and angular momentum conservations

Using Eq. (5.21) and outer boundary condition $f'(r_s) \approx 0$ of the homogeneously collapsing core, we calculate its total core mass

$$\begin{aligned} M &= \int d^3R \rho = a^3(t) \rho_c(t) 4\pi \int_0^{r_s} r^2 dr f^3 \\ &= a^3(t) \rho_c(t) \frac{\lambda\gamma}{4(\gamma-1)} \frac{4\pi}{3} r_s^3, \end{aligned} \quad (5.28)$$

and total core angular momentum

$$\begin{aligned} J &= \int d^3R \rho j = a^5(t) \rho_c(t) \Omega(t) \frac{8\pi}{3} \int_0^{r_s} r^4 dr f^3 \\ &\approx a^5(t) \rho_c(t) \Omega(t) \frac{\lambda\gamma}{4(\gamma-1)} \frac{8\pi}{15} r_s^5. \end{aligned} \quad (5.29)$$

The total core mass and angular momentum conservation lead to the constants ²

$$a^3(t) \rho_c(t) = \text{const.}, \quad a^2(t) \Omega(t) = \text{const.}, \quad (5.30)$$

in the homologous collapsing process from the initial core density ρ_c^{in} to the final core density $\rho_c^{\text{fi}} = \rho_c^{\max}$.

The ratio of total core mass and angular momentum

$$J/M \approx (2/5) a^2(t) \Omega(t) r_s^2, \quad (5.31)$$

is constant in time, and proportional to the rotation parameter $\mathcal{A}^2 a^2(t) \Omega(t)$ (5.17) for $\mathcal{A}^2 = 2r_s^2/5$. Therefore, we will use the ratio J/M to characterize system rotation and mass energies. In our case, $J/M \ll 1$ for a slow-rotating system of the rotational energy being much smaller than mass-energy.

² $a^3(t) \rho_c(t) = (\kappa/\pi G)^{3/2}$ for $\gamma = 4/3$

6 Photon-pair sphere/jet energetic properties

6.1 Photon-pair sphere/jet temperature profiles

Based on the *adiabatic* approximation discussed in Sec. 5, we can use the “*local*” virial theorem (3.4) to obtain the baryon heat energy dF (3.2) and temperature T (3.4). As discussed in Sec. 4, the baryon heat energy is transformed into the thermal energy of a photon-pair plasma through hadronic photon production, resulting in a photon temperature T_γ given by Eq. (4.3). Using these relations, the centrifugal potential (5.17) and homologous solution (5.20), we derive

$$\begin{aligned} \frac{T_\gamma}{m} \approx & 0.21 \frac{(v_s^c)^2}{6} \left\{ \frac{1}{\gamma(\gamma-1)} \left[(7\gamma-6)f^{3(\gamma-1)} - \frac{\lambda}{6}\gamma r^2 \right] \right. \\ & \left. - \frac{1}{2}\mathcal{A}^2 a^2 \Omega r^2 \sin^2 \theta \right\}. \end{aligned} \quad (6.1)$$

The first term inside the braces corresponds to the gravitational potential energy contribution to the temperature. The second term accounts for the rotational energy’s influence, which decreases the photon-pair plasma temperature due to the repulsive nature of the centrifugal potential ϕ_c acting against gravitational collapse. For $\theta \neq 0$, the photon-pair temperature T_γ becomes smaller, compared with non-rotating cases $\Omega = 0$.

The expression for T_γ highlights the interplay between the gravitational and centrifugal potentials in determining the thermal energy distribution of the photon-pair plasma during the homologous collapse of the rotating stellar core.

At the end of the homologous collapse $t = t_{\text{final}}$, the core’s central density reaches its maximum value $\rho_c = \rho_c^{\text{max}}$, and the sound speed squared is $(v_s^c)^2 = 1/3$, the produced photon-pair plasma forms an axial symmetric jet, described in the cylindrical coordinates. For illustration, we use the parameters, we use parameters $(\gamma, \lambda_m) = (1.23, 8 \times 10^{-5})$ (5.22) (the blue case) and $\mathcal{A}^2 a^2 \Omega = 0.05$, indicating a small centrifugal potential ϕ_c .

In Fig. 3, we plot the photon-pair plasma temperature T_γ for the non-rotating case $\Omega = 0$ and rotating cases $\Omega(t) \neq 0$. The maximal temperature is located at the centre $r = 0$. The vanishing temperature $T_\gamma(r, \theta) = 0$ determines the photon-pair sphere radius $r_\gamma < r_s$ or the jet boundary

$$r_\gamma^j(\theta) \leq r_\gamma, \quad R_\gamma^j(\theta) = a(t)r_\gamma^j(\theta). \quad (6.2)$$

The photon-pair sphere volume V_γ is larger than the photon-pair jet volume V_γ^j , see Fig. 4. In the rotating case, we plot the jet boundary $r_\gamma^j(\theta)$ in Fig. 5. As a self-consistency check, we find that the baryon temperature T and photon temperature T_γ are much smaller than baryon mass ($T_\gamma \approx 0.21T \ll m$). It fills the condition for applying the virial theorem (3.2).

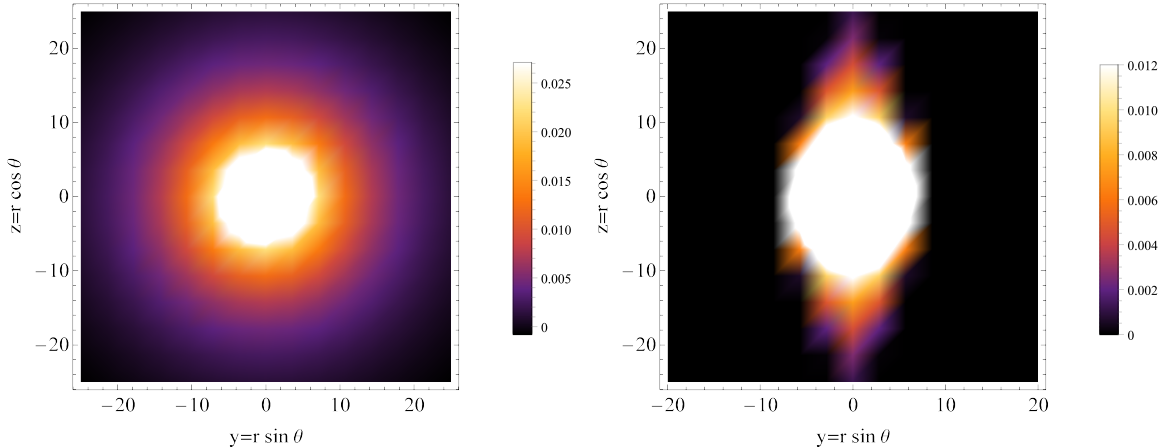


Figure 3. Colours online. Using results (6.1) for maximal sound velocity $(v_s^c)^2 = 1/3$, we plot the temperature T_γ/m in the cylindrical coordinates $y = R \sin \theta$ and $z = R \cos \theta$, where the θ is the zenith angle. The temperature unit is of typical baryon mass $m \approx 1$ GeV. The parameters are the *Blue* case parameters (5.22), and the initial conditions are (5.27). The upper panel is a non-rotating case $\mathcal{A}^2 a^2 \Omega = 0$. The lower panel is a rotating case of $\mathcal{A}^2 a^2 \Omega = 0.05$. The temperature vanishes at the photon-pair sphere radius r_γ or the jet boundary $r_\gamma^j(\theta)$. Both are smaller than the core outer radius r_s (5.22), see Fig. 1.

6.2 Photon-pair sphere/jet density and size profiles

We use photon productions (4.1) and (4.2) by baryon collisions to approximately obtain the photon-pair jet energy and number densities

$$\frac{\rho_\gamma}{\rho_0} \propto \left(\frac{T_\gamma}{m}\right)^4, \quad \frac{n_\gamma}{n_0} \propto \left(\frac{T_\gamma}{m}\right)^3, \quad (6.3)$$

in terms of photon-pair thermal temperature T_γ . The results show that the photon-pair energy density ρ_γ is in the range of $(10^{25} \sim 10^{30})$ ergs/cm³, and the number density n_γ is in the range of $(10^{37} \sim 10^{30})$ /cm³.

Using Eqs. (5.23), (5.24) and (5.26), we obtain the photon-pair sphere radius

$$R_\gamma = 3.06 \times 10^5 (3\gamma)^{-1/2} r_\gamma \left(\frac{\rho_0}{\rho_c^{\max}}\right)^{\frac{\gamma-1}{2}} \left(\frac{\rho_0}{\rho_c^{\text{in}}}\right)^{\frac{2-\gamma}{2}} \text{ (cm)}, \quad (6.4)$$

and the photon-pair jet boundary

$$R_\gamma^j(\theta) = 3.06 \times 10^5 (3\gamma)^{-1/2} r_\gamma^j(\theta) \left(\frac{\rho_0}{\rho_c^{\max}}\right)^{\frac{\gamma-1}{2}} \left(\frac{\rho_0}{\rho_c^{\text{in}}}\right)^{\frac{2-\gamma}{2}} \text{ (cm)}. \quad (6.5)$$

They are expressed as a function of initial core centre density ρ_c^{in} when a homologous collapse initiates. The photon-pair sphere size $R_\gamma \sim (10^7 \sim 10^{10})$ cm and the photon-pair cylindrical jet width $R_\gamma^j(\pi/2) \sim (10^6 \sim 10^9)$ cm.

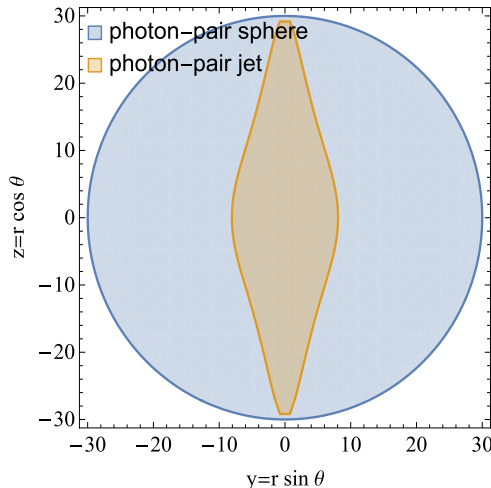


Figure 4. We compare the photon-pair sphere and jet boundaries of Fig. 3. The photon-pair sphere radius $r_\gamma \approx 30$ and $R_\gamma = a_{\min} r_\gamma \sim (10^7 - 10^{10})$ cm. The photon-pair jet boundary $r_\gamma^j(\theta)$ is given in Fig. 5.

Both sizes R_γ and R_γ^j are much larger than the photon mean-free path $\lambda_\gamma = (\sigma_\gamma n_\gamma)^{-1}$, namely $\sigma_\gamma n_\gamma R_\gamma \gg 1$ or $\sigma_\gamma n_\gamma R_\gamma^j \gg 1$. The photon-pair sphere/jet is deeply opaque. On the other hand, we find in Fig. 3 that the photon-pair sphere/jet temperature T_γ can be well above the critical energy threshold $2m_e = 1.02$ MeV of electron-positron (e^+e^-) pair production. The photon-pair sphere/jet energy density ρ_γ can be well above the critical energy density $\rho_e = m_e^4 = 5.93 \times 10^{-11} \rho_0$ of electron-positron pairs. This means the photons are quickly thermalised to form an electron-positron-photon plasma, as briefly discussed in Sec. 3. The photon-pair sphere/jet undergoes ultra-relativistic hydrodynamic expansion, which has been well-studied in the literature, and will not be studied in this article.

We compare the photon-pair sphere and jet boundaries in Fig. 4 and define the cylindrical jet angle θ_{jet} as the ratio

$$\theta_{\text{jet}} \approx \frac{R_\gamma^j(\theta = \pi/2)}{R_\gamma^j(\theta = 0)}, \quad R_\gamma^j(\theta = 0) = R_\gamma, \quad (6.6)$$

that characterizes the axial symmetric jet along the \hat{z} direction.

6.3 Photon-pair sphere/jet energy and spectrum peak

The total relativistic particle energy E_γ and number N_γ of the photon-pair sphere/jet can be obtained by numerically integrating the energy and number densities (6.3) over the photon-pair jet volume

$$V_\gamma^j = \int_{V_\gamma^j} d^3 R = a^3 \int_{V_\gamma^j} 2\pi r^2 dr \sin \theta d\theta. \quad (6.7)$$

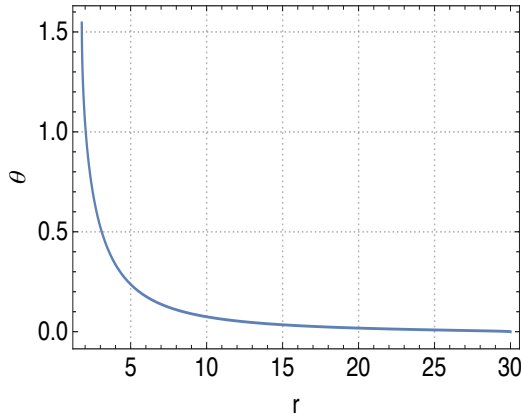


Figure 5. The photon-pair jet boundary $r_\gamma^j(\theta)$ shows that (i) $\theta \rightarrow 0$ and $r_\gamma^j(\theta)$ approaches to the radius $r_\gamma \approx 30$ of the photon-pair sphere; (ii) $\theta \rightarrow \pi/2$ and $r_\gamma^j(\theta)$ approaches to $r_\gamma^j(\pi/2) \approx 1$ of the photon-pair jet. The cylindrical jet width $R_\gamma^j = a_{\min} r_\gamma^j(\pi/2) \sim (10^6 - 10^8)$ cm. The jet angle (6.6) $\theta_{\text{jet}} \approx 1/30 \approx 1^\circ$.

We also compute the total baryon core mass

$$M = \int_{\text{core}} \rho d^3 R = \rho_c a^3 F_0, \quad (6.8)$$

and number $N = M/m$, where $F_0 \equiv \int_0^{r_s} 4\pi r^2 dr f^3$.

At the end of homologous collapse when the central sound velocity $v_s^c = \sqrt{1/3}$, we define integration

$$Y_n = 2\pi \int_{V_\gamma^j} \left(\frac{T_\gamma}{m} \right)^n r^2 dr \sin \theta d\theta \quad (6.9)$$

over photon-pair jet volume V_γ^j . From Eq. (6.3), we obtain the total energy and photon number of photon-pair jet systems

$$\frac{E_\gamma}{M} \propto \frac{Y_4}{F_0} \left(\frac{\rho_c^{\max}}{\rho_0} \right)^{4(1-\gamma)} \left(\frac{\rho_0}{\rho_c^{\text{in}}} \right)^{5-4\gamma}, \quad (6.10)$$

$$\frac{N_\gamma}{N} \propto \frac{Y_3}{F_0} \left(\frac{\rho_c^{\max}}{\rho_0} \right)^{3(1-\gamma)} \left(\frac{\rho_0}{\rho_c^{\text{in}}} \right)^{4-3\gamma}. \quad (6.11)$$

In addition, we define the mean temperature of the photon-pair sphere/jet as averaged value of T_γ (6.1) over photon-pair jet volume V_γ^j ,

$$\frac{\langle T_\gamma \rangle}{m} \propto \frac{Y_1}{Y_0} \left(\frac{\rho_0}{\rho_c^{\max}} \right)^{\gamma-1} \left(\frac{\rho_c^{\text{in}}}{\rho_0} \right)^{\gamma-1}, \quad (6.12)$$

which represents the characteristic temperature of the photon-pair sphere/jet. The photon-pair spectrum has a maximum at the peak energy $E_p \sim \langle T_\gamma \rangle$.

In Eqs. (6.10) and (6.12), we express total photon-pair energy E_γ and spectral peak E_p in terms of the initial core centre density $\rho_c^{\text{in}} = \rho_c(t_{\text{initial}})$ at the time t_{initial} when the core initiates homologous collapse. If the core mass M and baryon number N are fixed and conserved, the smaller initial core centre density ρ_c^{in} is, the more extended core mass density profile $\rho(r, t_{\text{initial}})$ is, i.e., the larger r_s is. As a consequence, more gravitational energy can be gained in collapse and converted to the photon-pair sphere/jet energy E_γ and number N_γ . In contrast, these quantities are also functions of the material binding energy parameter λ , the averaged thermal index γ and rotation parameter $J/M \propto \mathcal{A}^2 a^2 \Omega$. The rotation represents the repulsive reactions against gravitational collapse and energy gain.

For gravitational collapses from the initial core density $\rho_c^{\text{in}} \sim 10^{-6} \rho_0$ to the final one $\rho_c^{\text{max}} \sim 10 \rho_0$, we obtain

$$\begin{aligned} \frac{E_\gamma}{M} &\sim (2 \sim 5) \times 10^{-2}, & \frac{E_p}{m} &\sim (8 \sim 10) \times 10^{-5} \\ \frac{N_\gamma}{N} &\sim (1 \sim 3) \times 10, & R_\gamma &\sim (5 \sim 9) \times 10^8 \text{cm}, \end{aligned} \quad (6.13)$$

where the variations are due to the ranges of the parameters λ , γ and $J/M \propto \mathcal{A}^2 a^2 \Omega$. These quantities are conserved in the subsequent processes of the ultra-relativistic hydrodynamic expansion and internal/external collisions up to the transparent point when pairs annihilate and produce photons stream to detectors.

We have to point out that the photon-pair sphere/jet energetic properties (6.4,6.5) and (6.10,6.12) explicitly depend on the initial and final core central densities ρ_c^{in} and ρ_c^{max} . They characterize the gravitation gain and conversion to baryon kinetic energy and photon-pair thermal energy in gravitational collapses. These characteristics should also be held for gravitational collapses of non-spherical cores or coalescence of binary systems by introducing effective initial and final central densities $(\rho_c^{\text{in}})_{\text{eff}}$ and $(\rho_c^{\text{max}})_{\text{eff}}$ of the system.

By simplifying out (ρ_c^{in}) and (ρ_c^{max}) among Eqs. (6.4,6.5) and (6.10,6.12), we obtained theoretical correlations among the spectral peak E_p , total photon-pair energy E_γ and peak luminosity $L_\gamma \propto cR_\gamma^2 \langle T_\gamma \rangle^4 \propto cE_\gamma/R_\gamma$,

$$E_p \propto E_\gamma^\chi, \quad E_p \propto L_\gamma^{\frac{\chi}{\chi+1}}, \quad L_\gamma \propto E_\gamma^{1+\chi}, \quad (6.14)$$

with the unique positive parameter $\chi = \frac{\gamma-1}{4\gamma-5} \sim \mathcal{O}(1)$ ³. Although many intermediate processes have not been considered in this simplified model, the scaling laws (6.14) of GRBs' progenitors give an insight into the Amati and Yonetoku empirical relations, as well as the $L_\gamma \propto E_\gamma^{1+\chi}$ relation in a unified framework.

7 Long vs short GRBs by angular momentum and mass ratio

7.1 Trends of jet features varying with J/M

Based on the numerical results of Eqs. (6.9-6.12) and Fig. 4 for the parameters *Blue* case (5.22), using the initial condition (5.27), we calculate the photon-pair jet's angle

³It is an inverse of the original χ -definition [17]

J/M	θ_{jet}	E_p^j/E_p	E_γ^j/E_γ	L_γ^j/L_γ	R_γ^j/R_γ	N_γ^j/N_γ	V_γ^j/V_γ
0.001	13.2°	1.01	0.998	4.29	6.9/30	0.99	0.92
0.005	7.8°	1.25	0.99	7.24	4.1/30	0.97	0.63
0.01	6.3°	1.38	0.98	8.90	3.3/30	0.96	0.52
0.02	4.8°	1.52	0.97	11.6	2.5/30	0.93	0.42
0.03	4.2°	1.60	0.95	12.9	2.2/30	0.91	0.37
0.04	3.8°	1.66	0.94	14.1	2.0/30	0.89	0.33
0.05	3.4°	1.71	0.93	15.5	1.8/30	0.88	0.31
0.06	3.2°	1.74	0.92	16.2	1.7/30	0.86	0.29
0.07	3.1°	1.78	0.91	17.1	1.6/30	0.85	0.27
0.08	2.9°	1.81	0.90	18.0	1.5/30	0.84	0.26
0.09	2.7°	1.84	0.89	19.1	1.4/30	0.83	0.25
0.10	2.5°	1.86	0.88	20.3	1.3/30	0.82	0.24
0.15	2.1°	1.95	0.85	23.2	1.1/30	0.78	0.20

Table 1. For selected values of the rotation parameter $\mathcal{A}^2 a^2 \Omega$, i.e., the ratio J/M (5.31), we tabulate the jet angle θ_{jet} (6.6) and the ratios of the spectral peak E_p^j/E_p , total energy E_γ^j/E_γ , maximal luminosity $L_\gamma^j/L_\gamma \propto (E_\gamma^j/E_\gamma)(R_\gamma/R_\gamma^j)$, minimal size R_γ^j/R_γ , total particle number N_γ^j/N_γ and volume V_γ^j/V_γ between the photon-pair sphere and jet cases for comparisons. The photon-pair jet (with superscript j) and sphere quantities are given by Eqs. (6.4,6.11,6.12). Their ratios do not explicitly depend on the initial (final) core centre density ρ_c^{in} (ρ_c^{fi}) of gravitational collapses.

θ_{jet} , spectral peak E_p^j total energy E_γ^j and luminosity L_γ^j in comparison with the sphere counterparts. We select the rotation parameter $\mathcal{A}^2 a^2 \Omega \propto J/M$ values to gain an insight into the trends of how jet geometric and energetic features vary with the rotation angular momentum in Table 1.

7.2 A separatrix in angular momentum J/M

The photon-pair (approximate) sphere case represents one distinct class of the GRBs progenitors with small angular momenta ($J/M \gtrsim 0$), which are more likely for the cases of massive core collapses, relating to long GRBs. The photon-pair jet case with nontrivial angular momenta represents another distinct class of the GRBs progenitors, which are more likely for the cases of binary coalescence, relating to short GRBs. We will come back to this point later. In the cases of binary coalescence, systems have larger angular momenta J/M , where the core mass M should be an effective value of total system mass, the central density ρ_c (5.11) and its initial value (5.27) should be effective one. Since the separation between long and short GRBs classes is distinct, there must be a separatrix in angular momentum J/M . It occurs when the centrifugal potential ϕ_c is too large to be balanced by the gravitational potential ϕ and the material binding energy λ . Using the equilibrium equation (5.9) and gravitational potential ϕ balanced by the heat function h , we give a separatrix,

$$\phi_c \approx \frac{(v_s^c)^2 \lambda}{\gamma - 1} r^2 \quad \Rightarrow \quad J/M \propto (\mathcal{A}^2 a^2 \Omega)_{\text{sepa}} \sim \frac{\lambda}{3(\gamma - 1)} \approx \lambda \quad (7.1)$$

in this simplified model. When the repulsive rotation energy is larger than the material binding energy, namely $J/M > \lambda$, they are for the cases of binary coalescence. On the contrary, $J/M < \lambda$ are for the cases of massive core collapses. The real situation is much more complex.

7.3 Long vs short GRBs

The following qualitative observations and comments are in order from the trends of increasing or decreasing quantities as increasing angular momentum J/M in Table 1.

- (i) Due to the angular momentum and repulsive centrifugal potential increase, the gravitational energy gain becomes smaller. The ratios E_γ^j/E_γ and N_γ^j/N_γ are smaller than one but still in the order of unity, because most photons and pairs are produced at the centre ($z = 0, y = 0$) of the sphere and jet, see Fig. 3.
- (ii) The jet spectral peak E_p^j/E_p significantly increases up to twice larger than the spherical one, because the photon-pair energy density increases as the jet volume V^j decreases. As a result, the spectral peak E_p^j increases and total energy E_γ^j decreases as angular momentum increases. It gives a possible explanation for two distinct Amati relations $E_p \propto E_\gamma^\chi$ (6.14) respectively for long and short bursts' data scattering on the E_p - E_γ plane, see Fig 7 (right) of the reference [25], where two distinct Amati relations are observed for long and short bursts.
- (iii) The spectral peak E_p^j and the peak luminosity L_γ^j increase as angular momentum increases. It implies the Yonetoku relation $E_p \propto L_\gamma^{\chi/(\chi+1)}$ (6.14) is not the same for long and short bursts' data scattering on the E_p - L_γ plane, as shown in Figure 7 (left) of the reference [25].
- (iv) The jet and sphere size ratio $R_\gamma^j/R_\gamma \sim \mathcal{O}(10^{-1})$. It implies that long bursts duration $T_{90} \sim R_\gamma/(2c\Gamma^2)$ are about 10 times larger than short bursts $T_{90}^j \sim R_\gamma^j/(2c\Gamma_j^2)$. We assume hydrodynamic expansion Lorentz factors $\Gamma/\Gamma_j \sim \mathcal{O}(1)$, considering the obtained result $E_\gamma^j/E_\gamma \sim \mathcal{O}(1)$ in Table 1. It is qualitatively consistent with two classes of long (soft) and short (hard) bursts' data scattering on the E_p - T_{90} plane, see Figures 1 and 6 (up-right) of the reference [25]. However, the separatrix (7.1) of this simplified model cannot infer the separatrix $T_{90} \approx 1 \sim 2$ seconds between long GRBs (massive core collapses) and short GRBs (binary coalescence).
- (v) The trends of numerical results in Table 1 imply possibly positive or negative correlations between the jet angle θ_{jet} and burst duration T_{90}^j , spectral peak E_p^j , total energy E_γ^j , luminosity L_γ^j . Short GRBs should be more jetting than long GRBs.

These insights underscore the importance of considering rotational effects and jet dynamics in studying GRB spectra and their correlations.

8 Conclusion and remarks

To understand GRBs' jet progenitors, we adopt an adiabatic approximation and a simplified model to study photon-pair jets generated by the gravitational collapse of slowly rotating cores and binary systems. Our results qualitatively show photon-pair jets features: (i) the jet angle θ_{jet} relates to progenitor angular momenta and masses ratio J/M ; (ii) variation trends of GRBs' peak spectra, total energy and luminosity in terms of jet angle, positive and negative correlations among them; (iii) the distinction between short and long GRBs' properties is due to the different angular momentum of systems that undergo gravitational processes of binary coalescence or massive core collapse.

More theoretical studies and numerical simulations of massive rotating core collapse and binary coalescence are necessarily required to better understand the dynamics of massive rotating core collapse and binary coalescence. These studies will help refine our understanding of the photon-pair jet formation process and the resultant GRB properties.

The data analyses on possible correlations of GRBs' jet energetic, geometric and time-duration features are inviting. Systematic analyses of GRB data are required to explore possible correlations between jet energetics, geometric features, and time-duration characteristics. Understanding these correlations will provide deeper insights into the jet progenitor systems and the physical mechanisms driving GRBs.

In summary, our simplified model provides a qualitative framework to understand the generation of photon-pair jets from gravitationally collapsing systems. It highlights the significant role of progenitor angular momentum in determining the jet characteristics and, consequently, the observable properties of GRBs. Further theoretical and observational studies are crucial to validate and expand upon these findings, paving the way for a more comprehensive understanding of GRB jet progenitors and their evolution.

References

- [1] T. Piran, *The physics of gamma-ray bursts*, *Reviews of Modern Physics* **76** (2004) 1143 [[astro-ph/0405503](#)].
- [2] P. Mészáros, *Gamma-ray bursts*, *Reports on Progress in Physics* **69** (2006) 2259 [[astro-ph/0605208](#)].
- [3] E. Berger, *Short-Duration Gamma-Ray Bursts*, *Annual Review of Astron and Astrophys* **52** (2014) 43 [[1311.2603](#)].
- [4] P. D'Avanzo, *Short gamma-ray bursts: A review*, *Journal of High Energy Astrophysics* **7** (2015) 73.
- [5] P. Kumar and B. Zhang, *The physics of gamma-ray bursts & relativistic jets*, *Physics Reports* **561** (2015) 1 [[1410.0679](#)].

- [6] B. Zhang, *The Physics of Gamma-Ray Bursts*. Cambridge University Press, 2018, [10.1017/9781139226530](https://doi.org/10.1017/9781139226530).
- [7] R. Ruffini, R. Moradi, J. A. Rueda, L. Becerra, C. L. Bianco, C. Cherubini et al., *On the gev emission of the type i bdhn grb 130427a*, *The Astrophysical Journal* **886** (2019) 82 [[1812.00354](https://arxiv.org/abs/1812.00354)].
- [8] D. Lynden-Bell, *Statistical mechanics of violent relaxation in stellar systems*, *Mon. Not. Roy. Astron. Soc.* **136** (1967) 101.
- [9] D. Lynden-Bell and R. Wood, *The gravo-thermal catastrophe in isothermal spheres and the onset of red-giant structure for stellar systems*, *Monthly Notices of the Royal Astronomical Society* **138** (1968) 495.
- [10] S. Turbide, R. Rapp and C. Gale, *Hadronic production of thermal photons*, *Phys. Rev. C* **69** (2004) 014903 [[hep-ph/0308085](https://arxiv.org/abs/hep-ph/0308085)].
- [11] J. I. Kapusta, P. Lichard and D. Seibert, *High-energy photons from quark - gluon plasma versus hot hadronic gas*, *Phys. Rev. D* **44** (1991) 2774.
- [12] J. I. Kapusta, P. Lichard and D. Seibert, *High-energy photons from quark - gluon plasma versus hot hadronic gas*, *Nucl. Phys. A* **544** (1992) 485C.
- [13] P. B. Arnold, G. D. Moore and L. G. Yaffe, *Photon emission from quark gluon plasma: Complete leading order results*, *JHEP* **12** (2001) 009 [[hep-ph/0111107](https://arxiv.org/abs/hep-ph/0111107)].
- [14] C. Gale, Y. Hidaka, S. Jeon, S. Lin, J.-F. Paquet, R. D. Pisarski et al., *Production and elliptic flow of dileptons and photons in a matrix model of the quark-gluon plasma*, *Phys. Rev. Lett.* **114** (2015) 072301 [[1409.4778](https://arxiv.org/abs/1409.4778)].
- [15] Y. Hidaka, S. Lin, R. D. Pisarski and D. Satow, *Dilepton and photon production in the presence of a nontrivial polyakov loop*, *JHEP* **10** (2015) 005 [[1504.01770](https://arxiv.org/abs/1504.01770)].
- [16] P. Goldreich and S. V. Weber, *Homologously collapsing stellar cores*, *Astrophysical Journal* **238** (1980) 991.
- [17] S.-S. Xue, *Gravo-thermal catastrophe in gravitational collapse and energy progenitor of gamma-ray bursts*, *Journal of Cosmology and Astroparticle Physics* **2021** (2021) 044.
- [18] D. Lynden-Bell, *Homology in the evolution of cluster cores, cores, in dynamics of stellar systems*, *Proceedings from IAU Symposium no. 69, A. Hayli ed., Besancon, France, 9–13 September 1974*. **69** (1974) 27.
- [19] S. L. Shapiro, *The dissolution of globular clusters containing massive black holes.*, *Astrophysical Journal* **217** (1977) 281.
- [20] Y. Eriguchi and E. Mueller, *Equilibrium models of differentially rotating polytropes and the collapse of rotating stellar cores*, *Astronomy & Astrophysics* **147** (1985) 161.
- [21] T. Zwerger and E. Mueller, *Dynamics and gravitational wave signature of axisymmetric rotational core collapse.*, *Astronomy & Astrophysics* **320** (1997) 209.

- [22] H. Komatsu, Y. Eriguchi and I. Hachisu, *Rapidly rotating general relativistic stars. I - Numerical method and its application to uniformly rotating polytropes*, *Monthly Notices of the Royal Astronomical Society* **237** (1989) 355.
- [23] N. Stergioulas, *Rotating stars in relativity*, *Living Reviews in Relativity* **1** (1998) .
- [24] H. Dimmelmeier, J. A. Font and E. Müller, *Relativistic simulations of rotational core collapse I. Methods, initial models, and code tests*, *Astronomy & Astrophysics* **388** (2002) 917 [[astro-ph/0204288](#)].
- [25] A. Shahmoradi and R. J. Nemiroff, *Short versus long gamma-ray bursts: a comprehensive study of energetics and prompt gamma-ray correlations*, *Monthly Notices of the Royal Astronomical Society* **451** (2015) 126 [[1412.5630](#)].